2018

Tsunami Generation by Combined Fault Rupture and Landsliding

Perez del Postigo Prieto, Natalia

http://hdl.handle.net/10026.1/13604

Proceedings of the 7th International Conference on the
Application of Physical Modelling in Coastal and Port
Engineering and Science (Coastlab18)
Santander, Spain, May 22-26, 2018

Tsunami Generation by Combined Fault Rupture and Landsliding

NATALIA PEREZ DEL POSTIGO PRIETO[1], ALISON RABY[2], COLIN WHITTAKER[3], SARAH J. BOULTON[4]

1 School of Engineering, Plymouth University, United Kingdom, natalia.perezdelpostigoprieto@plymouth.ac.uk

2 School of Engineering, Plymouth University, United Kingdom, alison.raby@plymouth.ac.uk

3 Department of Civil and Environmental Engineering, The University of Auckland, New Zealand, c.whittaker@auckland.ac.nz

4 School of Geography, Earth and Environmental Sciences, Plymouth University, United Kingdom, sarah.boulton@plymouth.ac.uk

ABSTRACT

Tsunami generation and propagation mechanisms should be clearly understood in order to inform predictive models and improve coastal community preparedness. Experimental results, supported by mathematical models, could potentially provide valuable input data for standard predictive models of tsunami generation and propagation.

A unique set-up has been developed to reproduce a dual-source tsunami generation mechanism. The test-rig replicates a two-dimensional underwater fault rupture followed by a submarine landslide. The set-up was placed in a 20m flume of the COAST laboratory at Plymouth University. The aim of the experiments is to provide quality data for developing a parametrization of the initial conditions for tsunami generation processes which are triggered by a dual-source. The free surface elevation changes are investigated in relation to the fault rupture and landslide motions.

During the test programme, the water depth and the landslide density were varied. The position of the landslide model was tracked and the free surface elevation of the water body was measured. Hence tsunami characteristics of wave height, wavelength and propagation speed were determined. This paper provides a detailed description of the test rig and presents some preliminary results which highlight the performance of the test rig in terms of repeatability.

KEWORDS: Tsunami generation, submarine landslide, fault rupture, physical modelling, dual-source.

1   INTRODUCTION

Tsunami waves are impulsive waves generated by the sudden motion (uplift or downthrow) of the seafloor during a seismic event. The momentum from the ground motion is transferred, in the form of potential and kinetic energy into the water column, ultimately affecting the sea surface.

There are several natural phenomena capable of generating tsunamis, the most common being underwater earthquakes, landslides and volcanic eruptions. The subsequent tsunami wave characteristics are dependent on the triggering mechanism, with earthquakes and landslides the most researched tsunami sources. Many authors (e.g Hammack, 1972; Trifunac & Todorovska, 2002; Enet et al., 2003; Heller & Spinneken, 2013) have shown that source parameters control the wave generation. In the case of fault rupture, Hammack (1972) suggested that the initial free surface disturbance is proportional to the seafloor displacement (fault slip). It has conclusively been shown that the landslide geometry and density are the most relevant parameters that control the wave generation during experimental studies (e.g. Grilli & Watts, 1999; Heller & Spinneken, 2013, 2015; Watts & Grilli, 2003). It has also been suggested that solid landslide models over-estimate the wave amplitude in comparison to granular landslide models (Rzadkiewicz et al., 1997).

Earthquakes can trigger slope instability by shaking un-consolidated sediment, potentially resulting in a slope failure (landslide). If the earthquake has generated an impulsive wave, the slope failure could be due to either the earthquake or the tsunami wave (Wright & Rathje, 2003). In recent years, researchers have questioned the stand-alone earthquake source as tsunami trigger, suggesting slope failures as possible tsunami triggers. The 1998 Papua New Guinea tsunami was primarily triggered by a magnitude 7 earthquake. However, abnormally large tsunami run-ups of up to 15 m were observed in the Sissano Lagoon area, which could not be explained by the moderate earthquake magnitude. Moreover, numerical simulations of the event showed an inconsistent tsunami wave arrival time compared to the observational field data (Synolakis et al., 2002). Following a marine survey which provided evidence of a submarine slope failure, Synolakis et al. (2002) concluded that the 1998 PNG tsunami was caused by a large underwater slump. More recently, the 2011 Japanese tsunami (Tohoku) has been scrutinised, as evidence has been found to suggest that a local slump could have caused the unexpectedly large run-up heights of up to 40 m in the Sanriku area (Tappin et al., 2014).

Earthquake magnitude is proportional to the fault slip. Early studies of tsunami earthquakes approximated the initial water surface disturbance to be equivalent to the fault slip (Kajiura, 1981). Hammack (1972) determined empirical formulae to relate fault rupture characteristics to the generated wave properties. The current investigation aims to replicate the half-sine displacement time history from Hammack's study. However, the test-rig will perform the uplift motion by pulling the horizontal block vertically upwards from outside the water, rather than pushing the block up from beneath the test-rig, as in Hammack's experiments. A considerable amount of literature has been published on experimental studies of landslide generated tsunamis (e.g. Enet et al., 2003; Enet & Grilli, 2007; Hager, & Minor, 2008; Heller & Hager, 2010; Heller & Spinneken, 2012, 2013, 2015; Heller et al., 2016). These studies tested different landslides models, either solid blocks or granular, with various configurations (e.g. initial submergence, slide angle, landslide density), and results were then compared to numerical models. The existing research recognises the importance of the body geometry and density chosen to replicate the landslide and its initial conditions for wave generation (Heller & Spinneken, 2015; Philip Watts & Grilli, 2003). The research community recommended a benchmark configuration to facilitate comparison between studies (Grilli et al., 2002; Watts & Grilli, 2003), which has been adopted for the current investigation. Despite the physical modelling research done on earthquake generated tsunamis and landslide generated tsunamis, there are currently no experimental studies that deal with dual source tsunami generation.

This investigation aims to design and construct a novel dual source tsunami generation mechanism, which comprises a fault rupture and a landslide (partially-submerged and fully-submarine). Physical modelling of this dual mechanism will facilitate the investigation of complex interactions between the two sources and the water body. Results can be used to parametrise the fault rupture motion and geometry, the landslide shape and density, and the physical properties of the generated wave. These relationships can be applied to develop empirical models or to validate numerical simulations. One of the main challenges of this study has been achieving an acceptable degree of repeatability of the tsunami generation. Repeatability of the test rig motion is therefore the focus of this paper.

2 METHOD

2.1 Experimental set-up

The tsunami generation experiments were conducted in a 20 m long flume with a 0.6 m × 0.6 m section. The test rig, which comprises the square plate (fault rupture model), slopes and landslide model, partially sits on a grid where water is normally recirculated when the flume is being used for current generation (see Figure 1). The grid conveniently permits circulation of water when the uplift of the fault plate is performed. The wave generation was restricted to one-way wave propagation by a backwall as shown in Figure 1. Unfortunately, the generation area was only visible through a small observation window of 0.175 m by 0.6 m within the glass walls regions of the flume (as shown in Figure 2 and Figure 3).
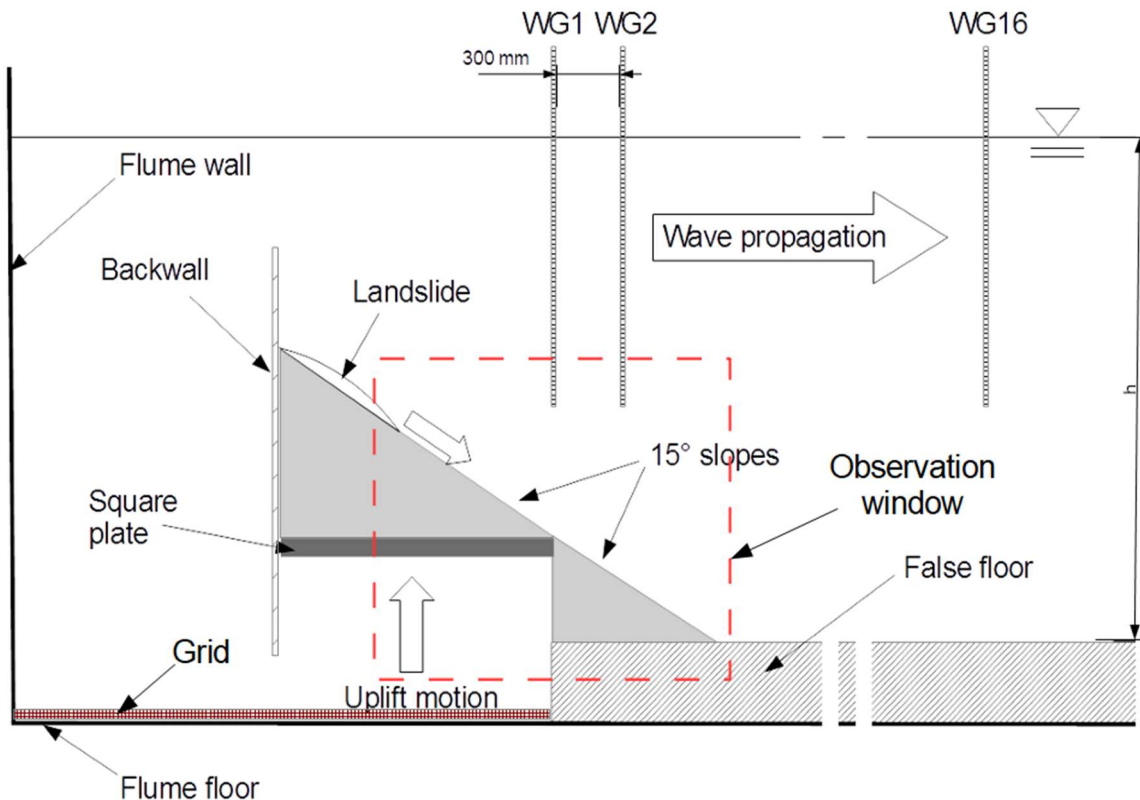

Figure 1 Schematic diagram of the experimental set-up showing the fault rupture and landslide models.

The test rig replicates two geological events: an (underwater) fault rupture followed by a submarine landslide. The fault rupture consists of a sudden uplift (up-thrust) of a plate, which is controlled by an electric actuator, which will be referred to as actuator throughout the text. A false floor was placed along the propagation area to provide sufficient clearance between the square plate and the grid and to maintain a constant depth (see Figure 1 and Figure 2).
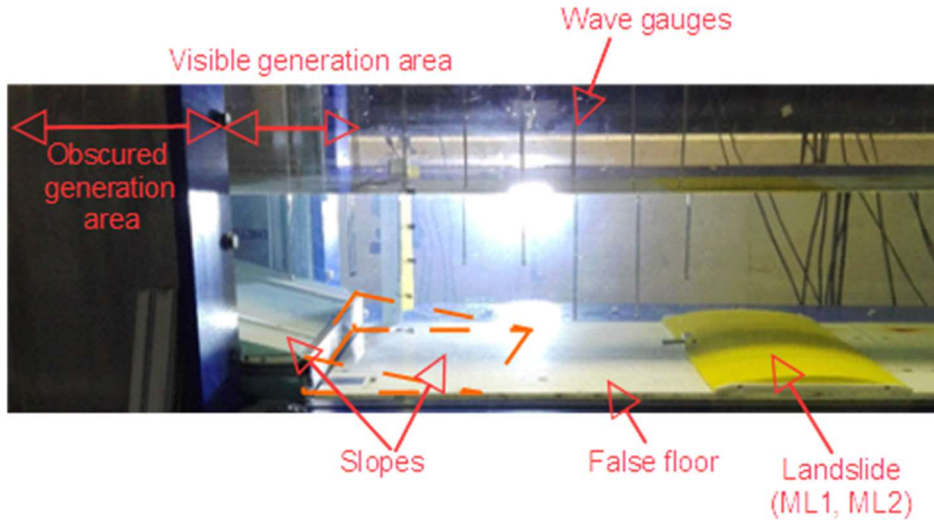

Figure 2 Experimental set-up during the preliminary tests. Red dashed lines represent the extension slope, added after the picture was taken.
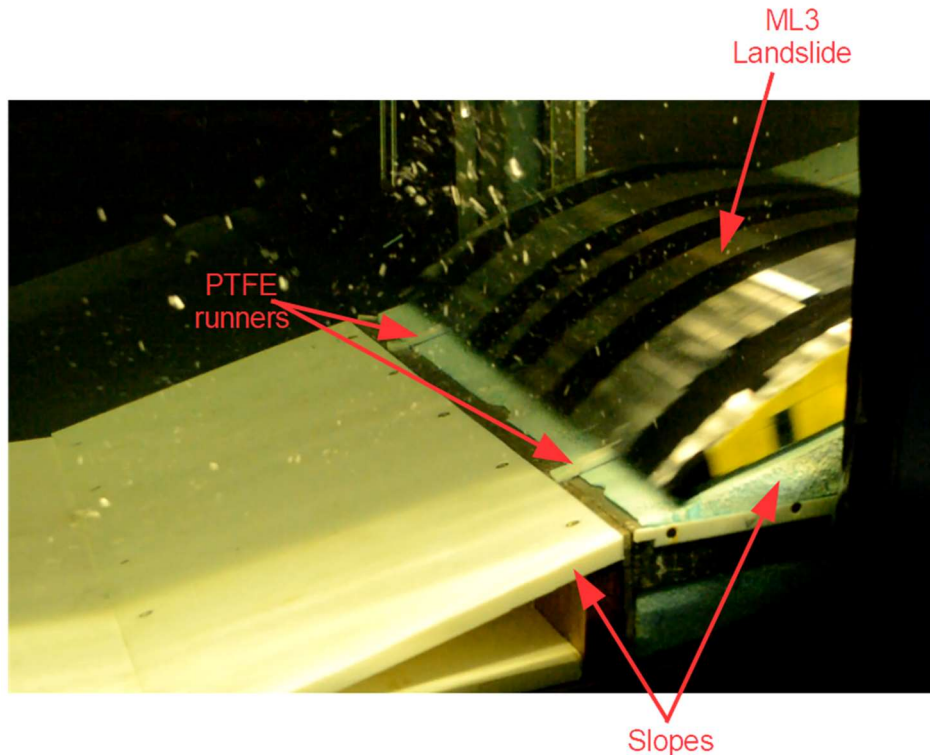

Figure 3 Observational window for Canon camera.

The square plate, which represents the uplifted seafloor, is attached to two vertical side plates that slide up and downthe flume walls on guide rails. The plate dimensions are 0.61 m long (similar to Hammack, 1972) by 0.6 m wide (corresponding to the flume width). The vertical side plates are joined by a cross-brace where the actuator is attached to perform the uplifting motion. All plates are made of aluminium, the horizontal plate is 5 mm thick and the remaining elements are 10 mm thick to ensure they do not flex during the uplift motion. Stiffening bars were added to the plate to prevent it from bending due to the large uplift force. Two fault ruptures were replicated: a horizontal plate uplift and an inclined plate uplift. The addition of an inclined plane to the test rig enables the landslide to be released, which slides down the slope guided on PTFE runners, as shown in Figure 3. The benchmark configuration (Grilli & Watts, 2002; Watts & Grilli, 2003) of a 15° slope and a rigid semi-elliptical landslide model were adopted. The uplift motion performed by the actuator in the current investigation aimed to reproduce the half-sine displacement time history of Hammack, (1972) with a maximum displacement of 60 mm displacement (see Figure 4).
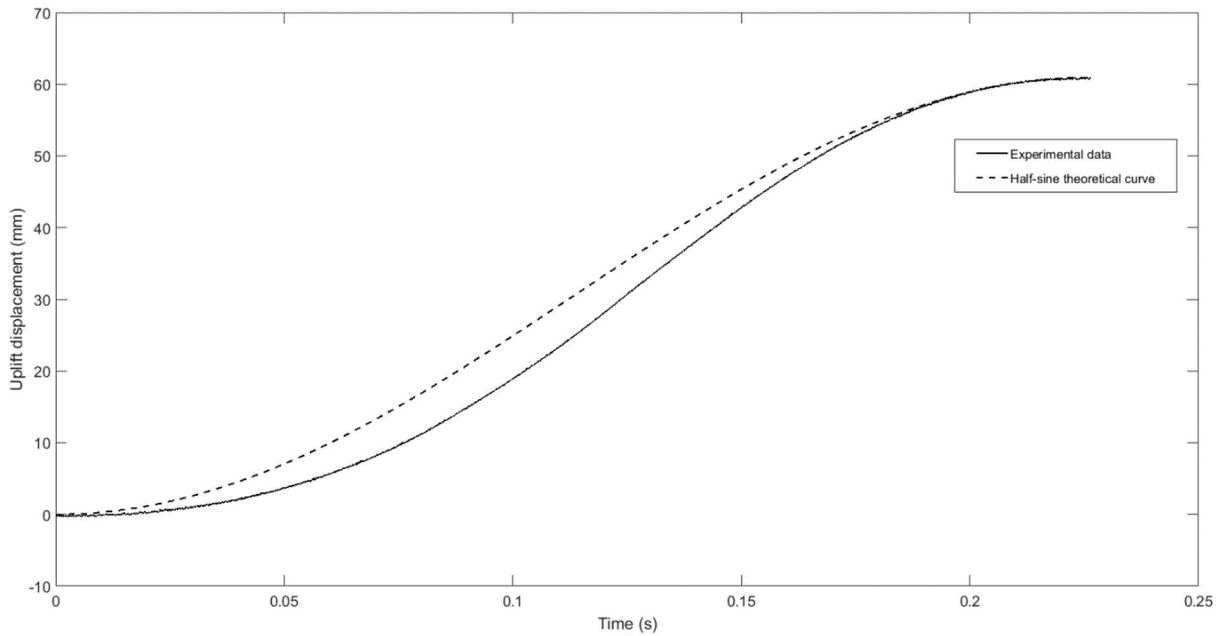
Figure 4 Experimental data for the uplift motion with a fitted half-sine curve as in Hammack, (1972).

The theoretical displacement, ς is

$$\varsigma = \frac{1}{2}\,A\sin\left(\omega t - \frac{\pi}{2}\right) + \frac{A}{2} \tag{1}$$

where A is the maximum amplitude of the uplift and $\omega = 2\pi/T$, where T is the sine wave period Figure 4 shows a reasonable fit between the experimental data and the theoretical curve. The amplitude and shape of both curves are similar, but the measured data lags the theoretical curve.

The landslide was represented by a semi-elliptical rigid body. Three landslide models with different densities were tested (see Figure 5). All models were made watertight to avoid the mass changing from run to run.
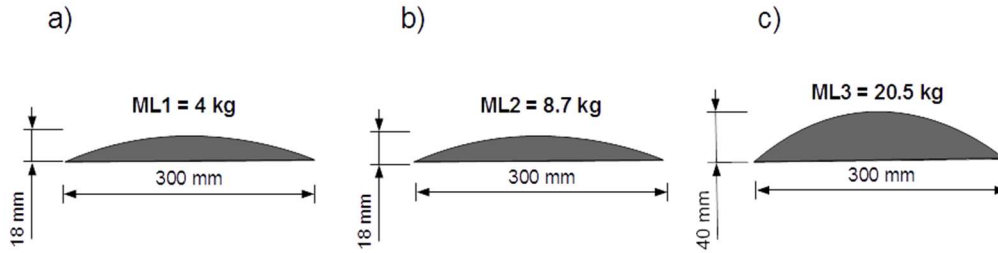

Figure 5 2D Sketch of landslide models: a) ML1, b) ML2, and c) ML3.

Models ML1 and ML2 were hollow with a sealable bottom hatch to enable lead to be inserted to vary the mass of the model whilst keeping the volume constant. A fixed bolt was inserted at the back end of the models as part of the release mechanism. The landslide was automatically released once the plate reached its maximum uplift displacement, at which point the bolt slid through a keyhole on the backwall. The landslide then moved solely under gravity. Model ML3 aimed to represent a granular landslide. The main feature of this model was its ability to change shape during its motion. This model consisted of twenty slices that were tested in different configurations, which were secured together with tape. To achieve the 20.5 kg weight, the landslide was constructed of a combination of stainless steel and aluminium. Two stainless steel rods were inserted through the uplift plate and the slope and fixed onto the flume floor. When the uplift was performed, both plate and slope moved through the rods, leaving them flush once the final distance was reached. This was when the ML3 is released. Details and results from the tests performed with ML3 will be reported on elsewhere.

2.2 Experimental Programme

A broad set of configurations were tested during each experimental campaign. Firstly, the fault rupture set-up was tested in four different configurations: horizontal plate uplift (HU), inclined slope uplift (IU), inclined slope uplift with moving landslide (IU-ML) and inclined slope uplift with fixed landslide (IU-FL). Moreover, different fault rupture uplift distances were performed: 0.6 m, 0.1 m and no displacement, in which case the landslide slid from the top of the slope under gravity only. Four water depths were used: 0.32 m, 0.27 m, 0.22 m and 0.165 m; in the last depth the ML3 landslide was only partially submerged. Throughout the various experimental campaigns, the different landslide models were tested on the IU configuration. The measured parameters were: free surface elevation time-history, uplift displacement time-history and landslide position.

For the repeatability study, the chosen test was the inclined slope uplift, with the moving landslide ML3, a 0.32 m water depth, and an uplift of 0.6 m (IU-ML3_320_60). The ML3 landslide model is the most complex and heaviest of the three and therefore the acceleration at which it travels would be largest. During the preliminary tests, this model was observed to have the most significant effect on the generated wave.

2.3 Instrumentation

Eight resistance wave gauges (WG) were placed along the centreline of the flume, approximately 0.3 m apart (see Figure 1), to record the free surface elevation changes. During the preliminary tests, the plate uplift was tracked with a Photron Fastcam SAH 64Gb recording at 500 fps. Simultaneously, the actuator's feedback was recorded. This feedback is the analog output from the encoder that reads the actuator motor response. Acquiring the video data allowed a comparison to the actuator's feedback displacement data, providing some confidence in the actuator values. An alternative approach to acquiring displacement data would be to undertake image processing of the high-speed camera frames; this would have been very time consuming for all tests performed. A comparison of the displacements obtained from the high-speed camera and the actuator feedback is shown in Figure 6.
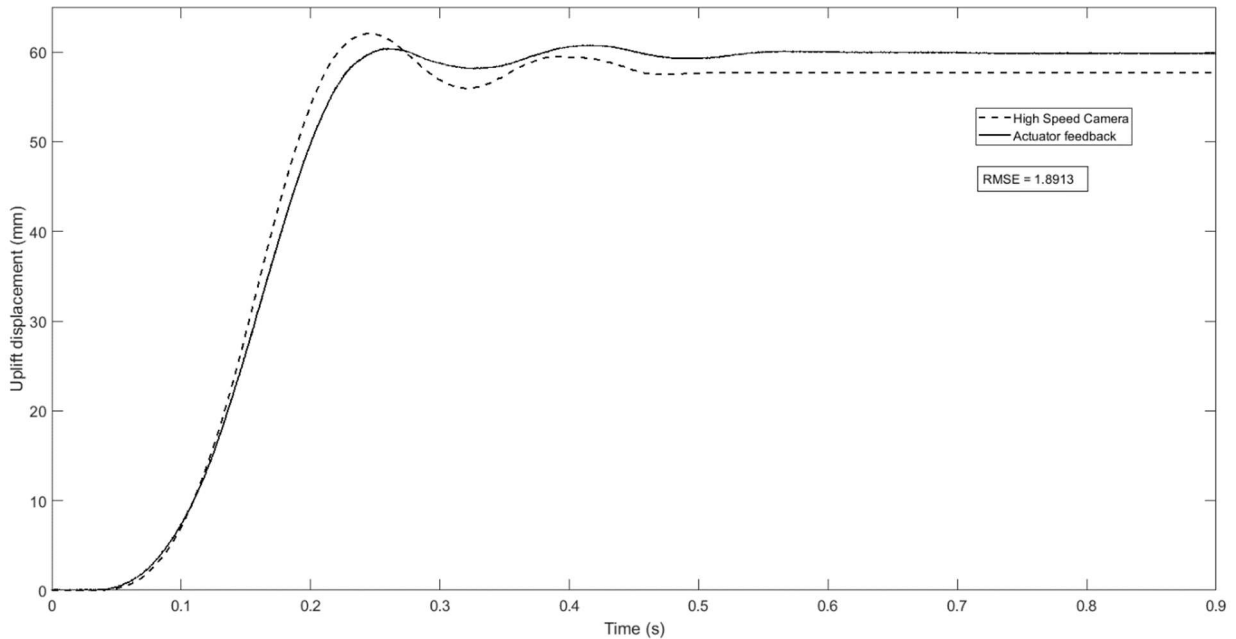

Figure 6 Actuator's feedback comparison with processed Photron footage.

The high-speed camera method involved manually tracking the plate through the video frames. Due to the computational load (i.e. large video files of up to 4Gb for less than 10 seconds of video) and time/ hardware constraints, the high-speed camera footage was not corrected in terms of image distortion. Therefore, the measurements obtained from the camera have to be considered as an approximation of the plate's position. However, the two methods agree with each other to within +/- 5 mm so the actuator's feedback is deemed reliable for estimating the uplift displacement. It is worth noting that the actuator feedback estimates the final displacement to be 60 mm, which coincides with the 60 mm vertical release position of the landslide.

The landslide motion was tracked with a Nikon Digital Camera D5200 recording at 50 fps. Owing to the limited observational area (see Figure 2), the camera was placed at an oblique angle towards the landslide (see Figure 7). This involved a meticulous geometric camera calibration to obtain the camera intrinsic, extrinsic, and distortion coefficients, which were computed using the *cameraCalibrator* Matlab toolbox. These were later applied to the recorded video frames to correct the lens distortion and convert the camera pixels to world units to obtain the real dimension of the tracked object. Full details on usage of the calibration toolbox and camera calibration can be accessed in MathWorks, 2017. N.B. It was more feasible to apply image correction to this orientation compared with the uplift motion orientation, due to more manageable file sizes (i.e. 20.1 Mb for 8s of video).
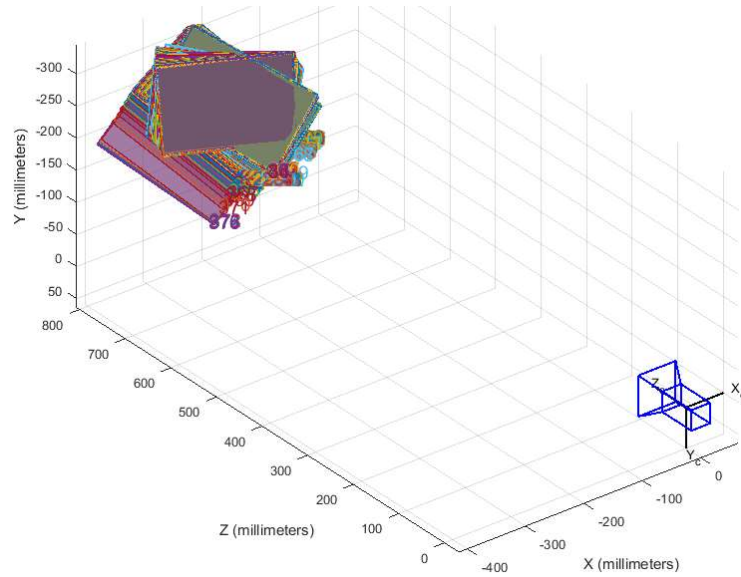
Figure 7 Canon camera position (bottom right) and recorded calibration frames (top left).

The video frames were corrected to an acceptable standard of 0.56 mean pixel error (0.148 mm) and the displacement-time histories of the landslide along the 15° slope were computed.

3   RESULTS AND DISCUSSION

This preliminary investigation aims to report on the repeatability of the novel dual source tsunami generator. In order to have a robust dataset for this investigation, runs of the same test were performed, recording video footage with the two cameras mentioned earlier, acquiring the actuator's displacement time histories and the free surface elevation time histories.

Figure 8 shows the uplift displacement time-histories obtained using the actuator feedback, recorded at 10 kHz. The actuator feedback measurements are remarkably repeatable with a standard deviation of 0.16 mm.
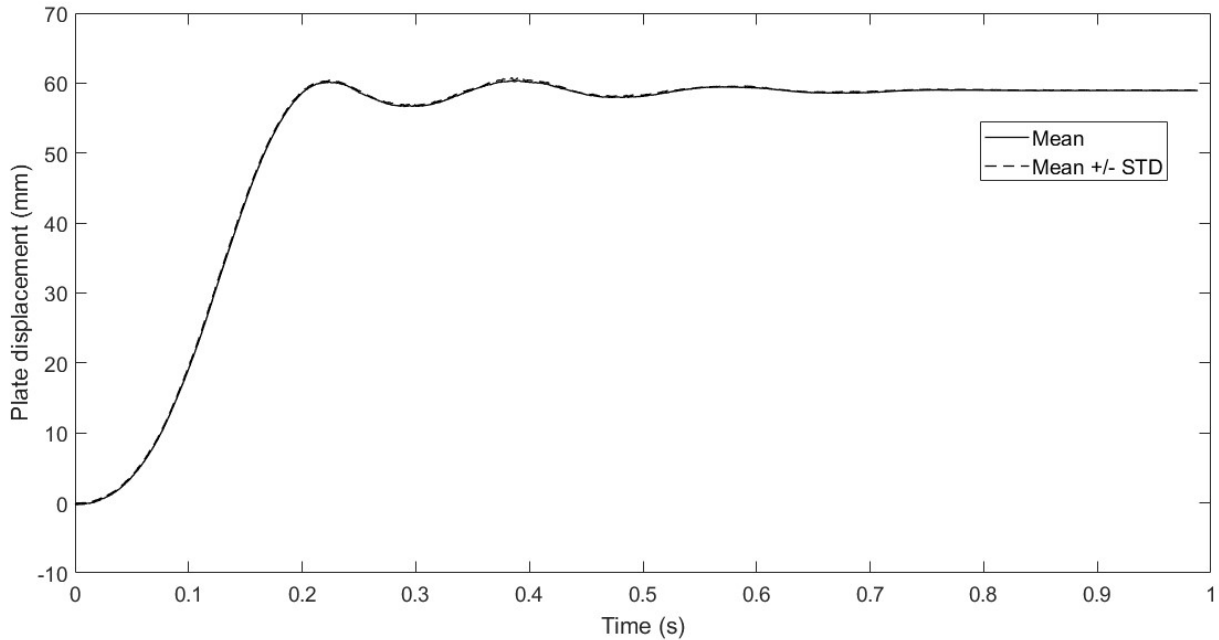

Figure 8 Repeatability of the uplift motion for nine runs of IU-ML3_320_60 test.

Photographs of the final position of the landslide using the Canon camera were used to determine the total distance travelled. Figure 9 shows the landslide model travel distance for nine sequential repeat tests of each of the three models.
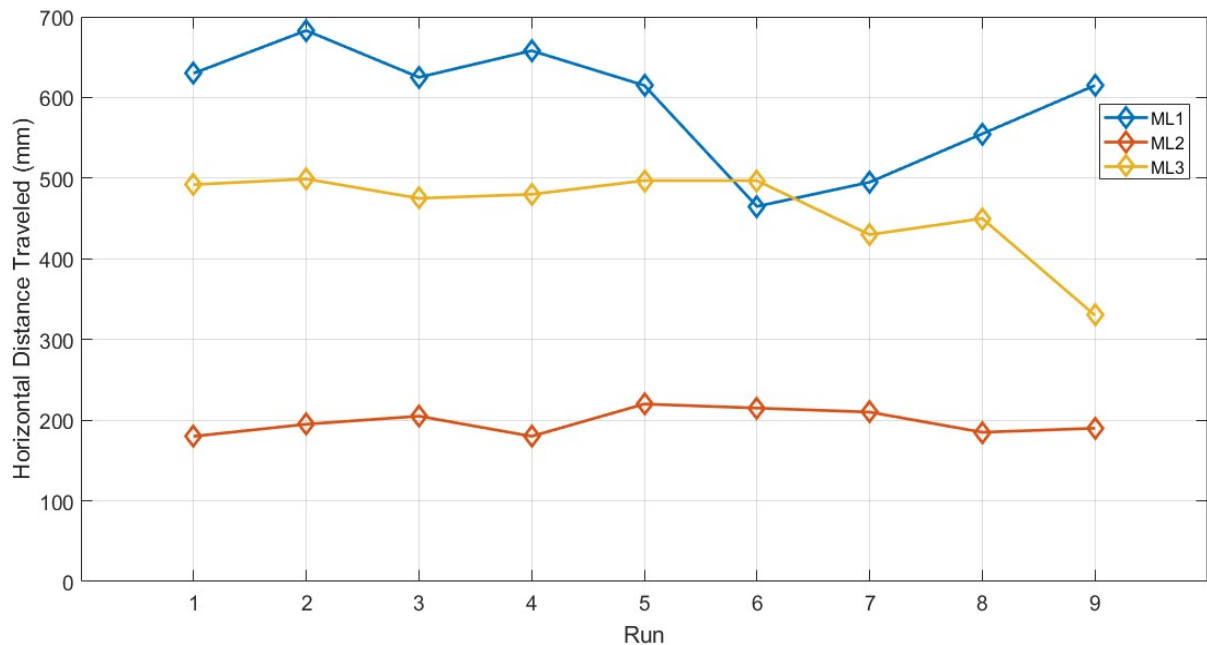
Figure 9 Landslide horizontal distance travelled for the three models ML1, ML2 and ML3.

Landslide model ML1, the lightest of the three aquaplaned, which resulted in the longest distance travelled as shown in Figure 9. However, the model was not completely watertight and its weight changed throughout the runs, which was reflected in a highly variable distance travelled, as shown in Figure 9. This resulted in reduced repeatability with a standard deviation of 69 mm.Landslide model ML2 has the highest repeatability with a standard deviation of 14 mm, but it did not travel very far (see Figure 9). Due to its weight (8.7 kg) being more than double the weight of the ML1 model, it did not aquaplane. The landslide stopped as soon as it reached the horizontal plane, sitting partially on the slope. Landslide model ML3 shows reasonable repeatability, with a standard deviation of 52 mm. It was observed to move laterally once it left the slope, which may explain the variability of the final distance travelled (see Figure 9).

In Figure 10 all three landslide cases produce a crest-led waveform, where the crest amplitudes decrease with increasing landslide weight. The crest is followed by a significant trough, the size of which increases with landslide weight. Figure 11 shows the free surface elevation time histories at location WG3. The effect of increasing weight on the crest amplitude is not as clear as in Figure 10 (crest amplitude decreases with weight from ML1 to ML2, but then increases from ML2 to ML3), however there is again a clear increase in trough amplitude with landslide weight.
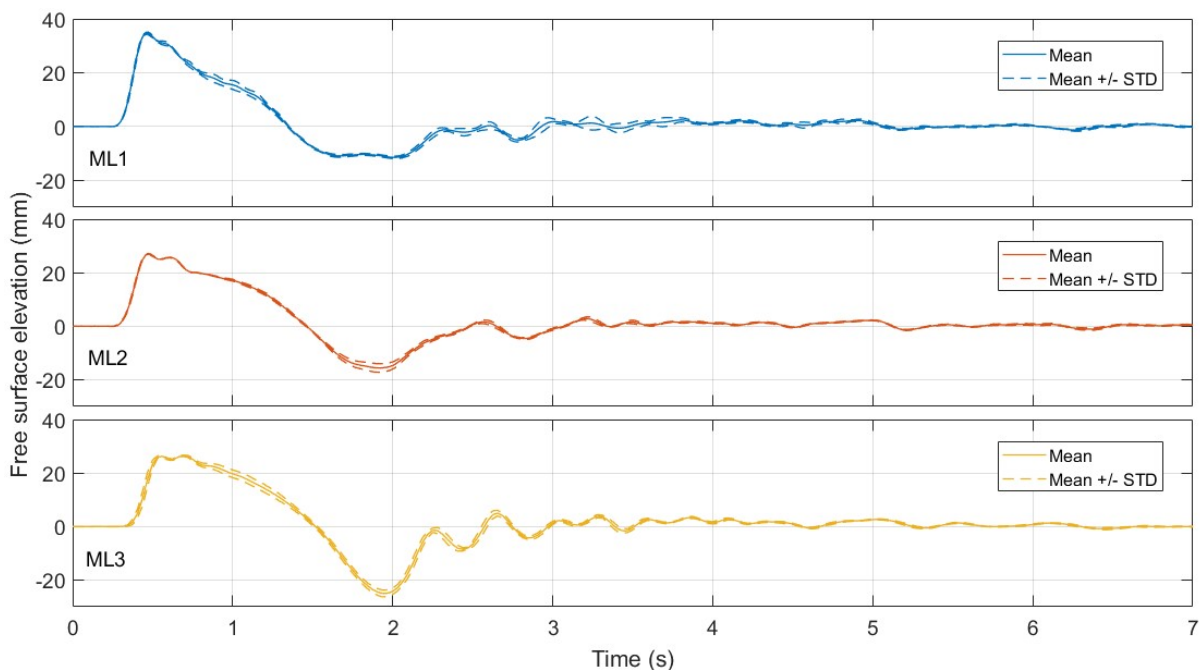

Figure 10 Free surface elevation repeatability for test IU_ML_320_60 at location WG1.
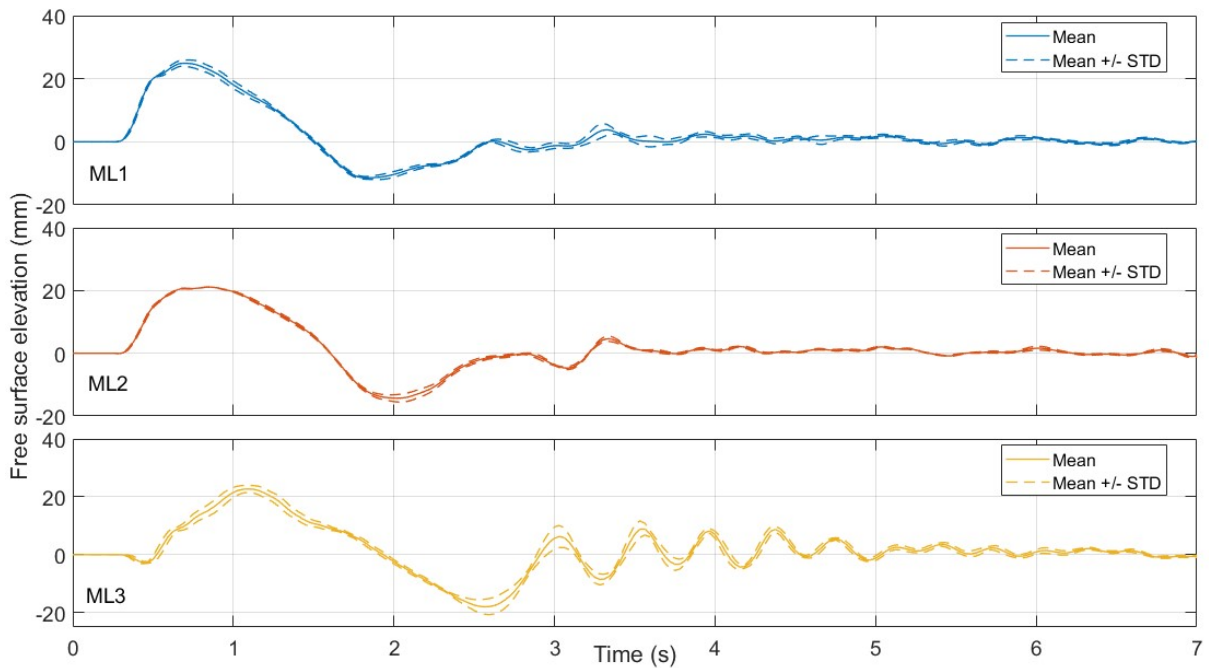
Figure 11 Free surface elevation repeatability for test IU_ML_320_60 at location WG3.

Figure 10 and Figure 11 present the standard deviations of the free surface elevation time-histories for 9 runs of test IU-ML with each of the three models, at locations WG1 (0 m) and WG3 (0.9 m), respectively. Table 1 summarizes the standard deviations for the three cases at locations WG1 and WG3. Both figures show an exceptional degree of repeatability. Owing to the construction of model ML3, its shape changed slightly throughout the runs as the tape stretched. This might have affected the landslide motion, which is reflected in the standard deviations values for ML3 (Table 1), and the effect on the generated wave. Despite these limitations, it can be concluded that the free surface elevation measurements are remarkably repeatable and can be used for further analysis, including for comparisons and validations with other studies.

Table 1. Standard deviations (in mm) for free surface elevation measurements
(IU_ML_320_60) for each landslide model at locations WG1 and WG3.

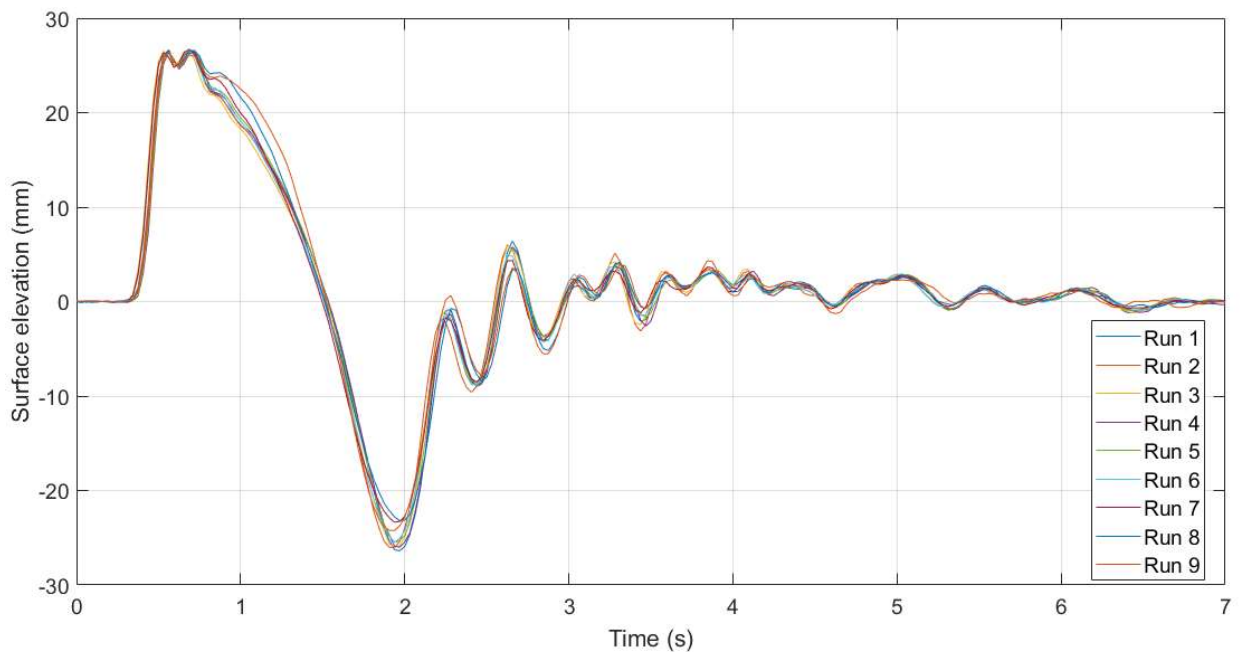|	ML1	ML2	ML3
WG1	0.22	0.35	0.51
WG3	0.22	0.34	0.89

Figure 12 Free surface elevation time histories at location WG1 for nine runs of test IU-ML3_320_60.

8

In Figure 12 all the nine runs show close alignment of wave peaks and troughs, but allowing slight variations in the amplitude (approximately +/- 5mm). This supports evidence for the remarkable repeatability of the free surface elevation measurements for experiments performed.

4   CONCLUSION

The current investigation was undertaken to design a novel dual source tsunami generation test rig and evaluate its level of repeatability. Experiments confirmed that the performance of the test rig was exceptionally repeatable and the data was acquired with a high degree of repeatability. The major limitation of this study was the difficulty of recording the landslide motion along the slope, which was restricted by a reduced observational area as described previously. However, the landslide horizontal distance travelled was noted. Repeatability was reasonable but less so for the lighter landslide model (ML1) which also suffered problems of aquaplaning and water ingress affecting its weight.

Notwithstanding these limitations, this is the first experimental study that has replicated a dual source tsunami generation mechanism. The repeatability of the test rig motions and resulting data lays the groundwork for further study of the acquired data. Findings from this study contribute to our understanding of tsunami wave generation by both earthquakes and landslides. By varying sources parameters and water depths, different scenarios can be replicated. Different configurations of the test rig will help understand the role of each source to the wave generation, enabling a complete parametrisation of the process. Furthermore, the high-quality data produced can be used for numerical model validation and empirical studies.

REFERENCES

Grilli, S. T., Vogelmann, S., & Watts, P. (2002). Development of a 3D numerical wave tank for modeling tsunami generation by underwater landslides. *Engineering Analysis with Boundary Elements*, *26*(4), 301–313.

Grilli, S. T., & Watts, P. (1999). Modeling of waves generated by a moving submerged body . Applications to underwater landslides, *23*, 645–656.

Hammack, J. L. (1972). *Tsunamis-a Model of Their Generation and Propagation*. California Institute of Technology.

Heller, V., & Hager, W. H. (2010). Impulse product parameter in landslide generated impulse waves. *Journal of Waterway, Port, Coastal, and Ocean Engineering*, *136*(June), 145–155. http://doi.org/10.1061/(ASCE)WW.1943-5460.0000037

Heller, V., & Spinneken, J. (2013). Improved landslide-tsunami prediction: effects of block model parameters and slide model. *Journal of Geophysical Research: Oceans*, *118*(3), 1489–1507.

Heller, V., & Spinneken, J. (2015). On the effect of the water body geometry on landslide-tsunamis: Physical insight from laboratory tests and 2D to 3D wave parameter transformation. *Coastal Engineering*, *104*(August 2016), 113–134. http://doi.org/10.1016/j.coastaleng.2015.06.006

Kajiura, K. (1981). Tsunami energy in relation to parameters of the earthquake fault model. *Bulletin of the Earthquake Research Institute*, *56*, 415–440.

Philip, W., Fumihiko, I., Aaron, B., & T., G. S. (2002, February 13). Benchmark Cases for Tsunamis Generated by Underwater Landslides. *Ocean Wave Measurement and Analysis (2001)*. http://doi.org/doi:10.1061/40604(273)152

Pzadkiewicz, S. Assier and Mariotti, C. (1997). Numerical simulation of submarine landslides and their hydraulic effects. *Journal of Waterway, Port, Coastal & Ocean Engineering*, *123*(4), 149.

Synolakis, C. E., Bardet, J.-P., Borrero, J. C., Davies, H. L., Okal, E. A., Silver, E. A., … Tappin, D. R. (2002). The slump origin of the 1998 Papua New Guinea Tsunami. *Proceedings of the Royal Society A: Mathematical, Physical and Engineering Sciences*, *458*(2020), 763–789. http://doi.org/10.1098/rspa.2001.0915

Tappin, D. R., Grilli, S. T., Harris, J. C., Geller, R. J., Masterlark, T., Kirby, J. T., … Mai, P. M. (2014). Did a submarine landslide contribute to the 2011 Tohoku tsunami? *Marine Geology*, *357*, 344–361. http://doi.org/10.1016/j.margeo.2014.09.043

Trifunac, M. D., & Todorovska, M. I. (2002). A note on differences in tsunami source parameters for submarine slides and earthquakes. *Soil Dynamics and Earthquake Engineering*, *22*(2), 143–155. http://doi.org/http://dx.doi.org/10.1016/S0267-7261(01)00057-4

Watts, P., & Grilli, S. T. (2003). Tsunami Generation By Submarine Mass Failure. Part I: Wavemaker Models. *Submitted J. Waterway Port Coastal and Ocean Engineering*.

Watts, P., & Grilli, S. T. (2003). Underwater Landslide Shape , Motion , Deformation , and Tsunami Generation. *International Offshore and Polar Engineering Conference*, *5*, 364–371.

Wright, S. G., & Rathje, E. M. (2003). Triggering Mechanisms of Slope Instability and their Relationship to Earthquakes and Tsunamis. In J.-P. Bardet, F. Imamura, C. E. Synolakis, E. A. Okal, & H. L. Davies (Eds.), *Landslide Tsunamis: Recent Findings and Research Directions* (pp. 1865–1877). Basel: Birkhäuser Basel. http://doi.org/10.1007/978-3-0348-7995-8_5